Solution-Processable Ultrathin Black Phosphorus as an Effective Electron Transport Layer in Organic Photovoltaics

Shenghuang Lin, Shenghua Liu, Zhibin Yang, Yanyong Li, Tsz Wai Ng, Zaiquan Xu,

Qiaoliang Bao, Jianhua Hao, Chun-Sing Lee, Charles Surya, Feng Yan, Shu Ping Lau**

((S. H. Lin and S. H. Liu contributed equally to this work))

S. H. Lin, S. H. Liu, Z. B. Yang, Y. Y. Li, Prof. J. H. Hao, Prof. F. Yan, Prof. S. P. Lau
Department of Applied Physics, The Hong Kong Polytechnic University, Hung Hom, Kowloon, Hong Kong (China)
E-mail: *apsplau@polyu.edu.hk*, *apafyan@polyu.edu.hk*

S. H. Lin, Z. Q. Xu, Prof. Q. L. Bao
Institute of Functional Nano and Soft Materials (FUNSOM), Jiangsu Key Laboratory for Carbon-Based Functional Materials and Devices, and Collaborative Innovation Center of Suzhou Nano Science and Technology, Soochow University, Suzhou 215123, P. R. China

Prof. Q. L. Bao
Department of Materials Science and Engineering, Monash University, Clayton, VIC 3800, Australia

T. W. Ng, Prof. C. –S. Lee
Center of Super-Diamond and Advanced Film (COSDAF) and Department of Physics and Materials Science, City University of Hong Kong, Hong Kong, P. R. China

Prof. C. Surya
Department of Electronic and Information Engineering, The Hong Kong Polytechnic University, Hung Hom, Kowloon, Hong Kong, P. R. China

Keywords: ((black phosphorus, solution-processable, electron transport layer, organic photovoltaics))

Abstract

Two-dimensional (2D) van der Waals crystals, possessing excellent electronic and physical properties, have been intriguing building blocks for organic optoelectronic devices. Most of the 2D materials are served as hole transport layers (HTLs) in organic devices. Here, we report that solution exfoliated few layers black phosphorus (BP) can be served as an effective electron transport layer (ETL) in organic photovoltaics (OPVs) for the first time. The power conversion efficiencies (PCEs) of the BP-incorporated OPVs can be improved to 8.18% in average with the relative enhancement of 11%. The incorporation of BP flakes with the optimum thickness of ~ 10 nm can form cascaded band structure in OPVs, which can facilitate electron transport and enhance the PCEs of the devices. Our study opens an avenue in using solution exfoliated BP as a high efficient ETL for organic optoelectronics.

1. Introduction

Two-dimensional (2D) van der Waals crystals have attracted much attention around the world [1-3] due to its potential in high performance electronic and optoelectronic devices [4-16]. In particular, 2D transition metal dichalcogenides (TMDs) have demonstrated a wide range of applications, including field effect transistors (FETs) [9], light-emitting diodes (LEDs) [10], photodetectors [11], and organic photovoltaics (OPVs) [17-20]. For a conventional OPV, the transparent anode (e.g., indium tin oxide, ITO) is usually coated with a hole transport layer (HTL), which must be a p-type material with a wide band gap [17]. Thus it can block electrons but transport holes, in order to minimize carrier recombination [18]. Among the HTL materials, conventional solution-processable PEDOT:PSS, which can minimize the detrimental effect of ITO electrode and align the energy barrier between the active layer and ITO, has been predominantly used as an anode modifier [19]. However, PEDOT:PSS is usually replaced by other inorganic materials (e.g., V_2O_5 [20], MoO_3 [21] and NiO [22]) to avoid eroding the ITO electrodes and to obtain higher power conversion efficiencies (PCEs). It should be noted that low-cost, solution processable and roll-to-roll processed OPVs cannot be satisfied with the cost-intensive preparation process of such inorganic oxides. Therefore, researchers have paid much attention to search for alternative materials to replace inorganic oxides. Solution-processed 2D materials, including graphene oxide (GO) [23-26], WS_2 [27], MoS_2 [28-31], WS_2/MoS_2 [32] and TaS_2 [33], have been demonstrated to be suitable for HTL which could enhance the PCEs of the OPVs. However, it is scarce to utilize 2D materials for electron transport layer (ETL) in OPVs [34-36]. As an effective ETL, the material must be of low work function and high electron mobility, and could lower the work function of the cathode and transfer electrons from the active layer to the cathode efficiently[19].

Recently, mechanically exfoliated few-layer black phosphorus (BP) [37] has attracted significant attention due to its high carrier mobility (~1000 cm^2/Vs) and ambipolar property [38-40]. In addition, solution based ultrasonication method has been demonstrated to be an

effective approach to exfoliate BP into few layer flakes [41-43]. The field effect hole mobility of the solution-exfoliated BP flakes can reach ~50 $cm^2V^{-1}s^{-1}$ [41, 42] which is however significantly lower than that of the mechanically exfoliated BP FETs [38]. It is notable that the solution-processable BP can be conveniently integrated into organic optoelectronic devices, which has not been explored yet. Here we demonstrate that the solution-processed BP flakes can be served as an effective ETL in OPVs. The PCEs of the BP-incorporated OPVs can be enhanced by 11% in relative and the maximum average PCE can reach 8.18%. The incorporation of appropriate thickness of BP flakes in ETL can form cascaded band structure in the devices, which facilitates the electron transport and enhances the PCE of the devices.

2. Results and discussion

Ultrasonication method was employed to exfoliate bulk BP crystals to ultrathin flakes. Figure 1a and 1b show the crystal structure of the layered BP and the appearance of a BP crystal respectively. Various solvents such as ethanol, acetone, N-methyl-2-pyrrolidone (NMP) and iso-propyl alcohol (IPA) were used for the ultrasonication process to exfoliate BP. Figure 1b shows the photograph of the exfoliated BP in various solutions. The solutions were centrifuged at 4000 rpm for 60 min. The exfoliated BP in different solvents exhibit slightly different colors which are due to the variation in concentration of BP in the solvents. The concentration of the BP flakes in the solvent can be adjusted by tuning the centrifugation process (see Supporting Information, Figure S1).

Raman spectroscopy was used to characterize the drop-casted BP prepared in IPA solvent. The Raman spectra of the BP flakes on SiO_2/Si substrates at six different locations are indicated in the optical image as shown in Figure 2a. The inset shows the typical Raman spectrum of the BP flakes with vibrational modes of A^1_g (360 cm^{-1}), B_{2g} (438 cm^{-1}) and A^2_g (466 cm^{-1}). These modes are corresponding well to few-layer BP [38-40]. The mode at 521 cm^{-1} is attributed to Si substrate which is substantially higher than the BP modes, revealing the

ultrathin thickness of the BP layer. The positions of the three Raman peaks remain unchanged for the six locations as shown in Figure 2b. The intensity ratios of A^1_g/Si, B_{2g}/Si and A^2_g/Si in sites 1 and 2 are higher than those in other sites. Therefore, the BP flakes are thicker in sites 1 and 2 as compared with other sites. The Raman peak positions are very sensitive to the layer numbers for few layer BP flakes while less sensitive for thick flakes. Due to the relatively big thicknesses of our BP flakes (>2nm), the Raman peak positions only show tiny shifts at different sites, being similar to the case reported by Castellanos-Gomez *et al*. [37]. On the other hand, the non-uniformity of the layer numbers and strains in the BP flakes will broaden the peaks and decease the resolution of the peak position.[44]

The thickness profiles of the samples measured by atomic force microscopy (AFM) are depicted in Supporting Information (Figure S2a and S2b). The different locations are surveyed and represented by different colored lines. Figure S2c shows the thickness distribution of the BP flakes after measuring 15 locations. The thickness of the BP flakes prepared in IPA and ethanol solvents ranges from 1 nm to 21 nm, the most frequent thicknesses are between 2 to 7 nm. Figure S3 shows the UV (ultraviolet)-vis (visible)-NIR (near infrared) absorption spectra of the BP in IPA and ethanol solvents. There are three UV absorption peaks located at 218.8, 260 and 335.2 nm for BP in IPA, and two peaks located at 273 and 327 nm for BP in ethanol. The visible and NIR absorption bands between 400 and 900 nm are highlighted in blue and pink, respectively. It can be found that the optical absorbance is low in the high wavelength regime, which is similar to the previous work [43]. The reason of the different absorbance peaks of BP in IPA and ethanol could due to the difference in thickness and size distribution [43]. The spectra are broad covering from UV to NIR regions, revealing the potential in optoelectronic applications.

In order to explore the structural properties of the BP flakes, scanning transmission electron microscopy (STEM) was employed. The BP samples were firstly transferred onto carbon grids by drop casting (Figure 3a). Figure 3b shows the low magnification TEM image of the

BP flakes with various morphologies. Figure 3c reveal that some flakes are restacked to form thicker BP clusters as shown in the darker area. The individual BP flake with lateral size of about 100 nm is circled in red dot as indicated in Figure 3c. The atomic structure of the marked individual flake is further analyzed using high-resolution TEM (HRTEM) as shown in Figure 3d, revealing the BP flakes possessing periodical stacking sequence. The crystal plane spacing of the sample is ~0.21 nm, which corresponds to (002) crystal plane of orthorhombic phosphorus by ICDD-PDF: No.76-1963. Further TEM characterization of the BP samples can be found in Supporting Information (Figure S4a,b,c,e). The crystal planes such as (040) and (002) can be observed as shown in Figure S4d and f, respectively. The top inset of Figure 3d shows the energy dispersive x-ray (EDX) spectrum of the sample, which reveals P to be the only element besides C, O and Cu originated from the copper grid. The bottom inset shows the selected area electron diffraction (SAED) pattern from the surface of BP, revealing the high crystalline quality of BP with three distinguished red circles assigned to (002), (101) and (200) planes with lattice spacing of 0.21, 0.16 and 0.26 nm respectively. Figure 3e reveals the layered structure of a BP flake. The flake consists of 7 layers as determined by the HRTEM image as shown in Figure 3f, which also reveals the thickness of one atomic layer BP is ~0.52 nm. By combining the fast Fourier transform (FFT) pattern (top right) and the structural simulation viewed along *OX* axis (bottom right), the layered structure of BP is confirmed. Figure S5a shows the electron energy loss spectroscopy (EELS) of the sample at the phosphorus K and L edges. The EELS elemental mapping at the P-$L_{2,3}$ edge implies that the entire selected area consists of phosphorous atoms. The size distribution of the BP flakes in IPA and ethanol ranges from 50 to 200 nm as determined by TEM (Figure S5b).

The photoluminescence (PL) spectra of the BP in IPA and ethanol solutions are shown in Supporting Information (Figure S6). A strong broad PL peak at 0.94 eV can be observed in the BP prepared in both IPA (Figure S6a) and ethanol (Figure S6b). The broad PL emission peak correspondes to the bandgap of few layer BP (>3 layers) [45]. In addition to the strong and

broad emission peak, the PL spectrum of the BP solution in IPA also exhibits a few weak peaks at around 0.87 eV, 0.88 eV, and 0.90 eV. These emission peaks may be attributed to BP with other thicknesses. The normalized PL spectra of the BP in IPA solution as a function of time are shown in Figure S5c. The PL peak positions of the BP solutions remain unchanged after 35 days of storage time, indicating the high stability of the BP solution.

Next, we demonstrate the utilization of the solution exfoliated BP in OPVs as carrier-transport layers, including ETL and HTL. As solution processed BP flakes cannot make full coverage with a thin thickness on a substrate as evidenced by the poor conductivity of spin-coated BP films (Supporting information, Figure S7), it is difficult to utilize BP as a carrier-transport layer independently without using PEDOT:PSS or ZnO. Thus, we attempted to spin-coat BP onto PEDOT:PSS and ZnO layers to change the hole and electron transport behavior in OPVs, respectively. Two types of OPV devices with conventional and inverted structures shown in Figure 4a were fabricated [46-48]. Poly[4,8-bis[(2-ethylhexyl)oxy]benzo[1,2-b:4,5-b']dithiophene-2,6-diyl][3-fluoro-2-[(2-ethylhexyl)carbonyl]thieno[3,4-b]-thiophenediyl] (PTB7) and [6,6]-phenyl- C71-butyric-acid-methyl-ester ($PC_{71}BM$) were used as the p-type and n-type active layer materials, respectively. It is crucial to control the thickness of BP deposited on the ETL/HTL to optimize its enhancement in charge transfer, which is realized by spin coating BP in ethanol solution for different times. The ethanol solution is chosen because of its compatibility with PEDOT:PSS and ZnO films.

The current density-voltage (J-V) characteristics of the two types of OPVs with the incorporation of BP under different conditions are shown in Figure 4b and 4c. For conventional structure,[46] BP together with PEDOT:PSS as HTL gives rise to the decrease of the short-circuit current density (J_{sc}) and open-circuit voltage (V_{oc}), resulting in the degradation of power conversion efficiencies (PCE) of the devices. However, when BP is used on ZnO as the ETL in the inverted device,[48] obvious improvement of J_{sc} and PCE can be observed, as depicted in Figure 4c.

Detailed photovoltaic performances including average V_{oc}, J_{sc}, fill factor (FF), PCE and PCE enhancement parameters obtained from a group of devices were summarized in Table S1 and S2. For the conventional device structure, BP was coated onto the PEDOT:PSS layer for few times. With the increase of BP coating time to 3, the J_{sc} and V_{oc} decreased gradually from original 16.26 to 15.22 mA/cm^2, and 0.731 to 0.696 V, respectively, leading to the decrease of the PCE from 7.72% to 6.52% in average.

Interestingly, when BP was coated on the ZnO layer, it provided a positive effect on the performance of the inverted device. As shown in Table S2, the average PCE of the optimal OPVs with 3 times' coating of BP was improved to 8.18±0.05%, which corresponds to 11.0% relative enhancement in PCE in comparison with the efficiencies of control devices (7.37±0.20%). The increase of J_{sc} is the main contributor to the PCE improvement, while V_{oc} and FF have no significant change. In particular, compared to the control device, the devices with twice and three times' BP coating show the average J_{sc} increased from 17.31 to 18.05 and 18.81 mA/cm^2, respectively. The champion device obtained with 8.25% efficiency by 3 times' coating, resulting from J_{sc} of 18.78 mA/cm^2, V_{oc} of 0.72V and FF of 61.0%. However, further increase of the thickness of BP by 4 times' spin-coating can inversely decrease the average PCE to 7.94 ± 0.15%, which is mainly due to the decrease of FF by 59.2% in average. Normally, the thickness of an ETL should be very thin [19], otherwise a high series resistance of the device can be induced by the ETL, which will decrease the FF of the device. The average thicknesses of the BP films coated for 2, 3 and 4 times were characterized to be 6.4, 10.8 and 15.2 nm, respectively. Therefore, the ideal thickness of the BP-based ETL is about 10 nm, which is very similar to those of other 2D material-based charge transport layers [19].

The external quantum efficiency (EQE) measurements of the OPVs were subsequently conducted to illuminate the enhancement of the device performance. As depicted in Figure 5a, higher EQEs ranging from 350 - 500 nm were observed upon incorporation of BP into the inverted devices in comparison with the control devices. In particular, with 3 times' BP

coating, the EQE improvement arrives at the maximum value, which is consistent with the highest J_{SC} enhancement, as shown in Table S2. However, further increase of the BP thickness in the device by 4 time's coating cannot lead to the further increase of EQE anymore, as indicated in Figure 5a.

It is assumed that the different device performance resulting from BP as ETL or HTL in our OPVs could be related to the energy levels of the BP thin films. We utilized ultraviolet photoelectron spectroscopy (UPS) to examine the band structure of BP prepared by twice and 3 times' coating on high-doped Si substrates. The UPS spectra in Figure 5b show the secondary electron cutoff position of the BP deposited on the Si substrates. It is located at 17.4 eV with twice BP coating (black curve), while with 3 times' coating, the secondary electron cutoff of BP shifted to 17.2 eV (red curve), indicating a 0.2 eV downshift of the vacuum level of BP with the increase of the thickness. Meanwhile, the onset of the valence band (VB) maximum of BP is found at 5.0 eV (black curve, Figure 5c) with twice spin coating.[49] A 0.2 eV shift of VB for 3 times' coating of BP is observed and the onset is located at 4.8 eV. Based on the PL spectrum as shown in Figure S5, the average band gap of the BP is ~0.94 eV. We can calculate the bottom levels of the conduction band (CB) for the BP prepared with twice and 3 times coating to be 4.06 and 3.86 eV, respectively, which are close to the value in other reports [50, 51]. It is obvious that the coating time of the BP film will not influence the band structure. Considering that the BP flakes cannot completely cover the Si substrates especially for less coating time, the UPS curves may be influenced by the exposed substrates. Therefore, the data for the 3 time coating film are more reliable and thus adopted in the paper. The corresponding energy diagram of the OPV device with inverted structure is illustrated in Figure 5d. All of the energy levels of PTB7, $PC_{71}BM$ were chosen from the literature [38, 39]. It is notable that the inverted OPV has a cascaded band structure with the BP incorporation (both for twice and 3 times' coatings), which is favorable for efficient electron transport and can prohibit carrier recombination near cathodes. On the other hand, 3 times'

coating of BP can lead to better coverage of BP on a ZnO film than twice coating and thus better perform of the device can be obtained at this condition. On the contrary, for the incorporation of BP onto PEDOT layer in the conventional structure (Figure 4a), the mismatched band structure of the BP layer may trap holes and block the hole transport near the anode (See supporting information, Figure S8), leading to the decrease of J_{sc} and PCE.

It has been reported that the property of BP is very sensitive to its environment especially some gas molecules.[52] To confirm the stability of BP incorporation into OPVs, we measured the performance of the OPVs with the inverted structure immediately after the preparation and after the storage in air for ~60 days. As shown in Table S3, the device with BP exhibited a little decrease of PCE from 8.25% to 7.77% after the 2 month storage, revealing a degradation of -5.82%. In contrast, the PCE decreased from 7.64% to 6.93% with a degradation of -9.29% in terms of the OPV without BP incorporation. Therefore, solution-processed BP flakes sandwiched by other materials in OPVs and encapsulated by glass caps can show relatively good stability in air.

3. Conclusion

In summary, solution exfoliated BP flakes are utilized as ETL in OPVs for the first time and lead to pronounced enhancement of the device performance. The average PCE of the OPVs is enhanced by 11% relatively when compared to that of the control device, corresponding to the increase of PCE from 7.37% to 8.18%. We find that the incorporation of BP as ETL in the OPVs can result in a cascaded band structure, which is favorable for electron transport and can prohibit carrier recombination near the cathodes. The processing conditions have been optimized and the optimum thickness of the BP layer is about 10 nm. Moreover, BP incorporated in OPVs shows good stability in air due to the encapsulation of the devices and are thus suitable for practical applications in the future. Our study implies that the solution exfoliated BP is an ideal carrier transport material for high-performance and solution-

processable organic optoelectronic devices.

4. Experimental Section

Preparation of BP flakes: BP crystal was purchased from Smart Elements. About 20 mg of BP crystals was added into acetone (4mL), IPA (4mL), NMP (4mL) and ethanol (8 mL) solutions. The samples were ultrasonicated using an ultrasonic bath of 400 W at a temperature of 28 °C for 48 hrs. The obtained BP solution was centrifugaed with rates of 1000 - 4000 rpm for 60 min in order to remove larger particles. The BP solutions with different concentrations can be obtained by tuning the centrifugation rates.

Characterizations of BP flakes: Raman spectra were collected using a Horiba Jobin Yvon HR800 Raman microscopic system equipped with a 488 nm laser operating at 180 mW. The spot size of the excitation laser is ~1 μm. The AFM measurements were performed in a Veeco Dimension-Icon system with a scanning rate of 0.972 Hz. The PL measurement was carried out using an excitation laser of 808 nm. The structural properties of the BP samples were characterized by a Jeol JEM-2100F scanning transmission electron microscope (STEM) and energy dispersive X-ray (EDX) operated at 200 kV. Electrical measurements were performed at room temperature in ambient conditions using a probe station equipped with semiconductor property analyzers (Keithley 2400 & Keithley 2410). The devices were wire-bonded prior to electrical measurements.

Fabrication of solution-cast BP-based solar cell: OPVs with conventional and inverted stuctures were prepared by solution process as shown in Figure 4a. Patterned ITO/glass with a sheet resistance of 15 Ω/cm^2 was used as the substrates. The ITO substrates were cleaned by acetone, isopropyl alcohol and deionized water and then treated with O_2 plasma. For conventional device, a ~40 nm poly (3,4–ethylenedioxy thiophene): poly (styrenesulfonate) (PEDOT:PSS) layer was spin coated on ITO and annealed at 150 °C for 1 h. For another inverted structure, a ~40 nm ZnO layer was spin coated on ITO/glass and annealed at 200 °C

for 1 h. After that, BP ethanol solution was spin coated on the PEDOT:PSS or ZnO layers, followed by 70 °C annealing for 5 mins. The same coating processes were repeated by different times. Then PTB7/$PC_{71}BM$ (1:1.5 weight ratio) blend with the mixed solvent of chlorobenzene (CB) and 1,8-diiodoctane (DIO) (97:3 volume ratio) was spin-coated on the BP modified electrodes at 1500 rpm for 60 s in a N_2-filled glovebox, followed by slow drying process. Before electrode deposition, methanol was spin coated onto the active film at 2500 rpm for 60 seconds. Finally, a 20 nm thick Ca and a 100 nm Al electrode were sequentially deposited on the active layers of conventional OPVs by thermal evaporation. A 10 nm MoO_3 and 100 nm Ag were evaporated on the active layers of inverted devices. The areas of the active layers of all the devices were kept at 8.0 mm^2. All OPVs were encapsulated with glass caps in the glove box and then tested in air.

Characterization of BP-based solar cell: The *J-V* characteristics of the OPVs were measured by using a Keithley 2400 source meter under the illumination of 100 mW/cm^2 (Newport 91160, 300 W, solar simulator equipped with an AM 1.5 filter). The light intensity was calibrated with a standard silicon solar cell. The EQE spectra of the devices were measured with a standard system equipped with a xenon lamp (Oriel 66902, 300W), a monochromator (Newport 66902), a Si detector (Oriel 76175_71580), and a dual channel power meter (Newport 2931_C).

Supporting Information

Supporting Information is available from the Wiley Online Library or from the author.

Acknowledgements

This work was financially supported by PolyU grants (Project no. 1-ZE14) and the Research Grants Council (RGC) of Hong Kong, China (Project no. T23-713/11). One of the authors (SHL) acknowledges the support from the Postdoctoral Science Foundation of China (No.

7131701013), Hong Kong Scholars Program (No. G-YZ36) and the postdoctoral early development program of Soochow University (No. 32317156 & No. 32317267). Q. Bao acknowledges the support from 863 Program (Grant No. 2013AA031903), the youth 973 program (2015CB932700), and the NSFC grants (Grant No. 51222208, 51290273, 91433107).

.

Received: ((will be filled in by the editorial staff))
Revised: ((will be filled in by the editorial staff))
Published online: ((will be filled in by the editorial staff))

[1] K. S. Novoselov, V. I. Fal′ko, L. Colombo, P. R. Gellert, M. G. Schwab, K. Kim, *Nature* **2012**, *490*, 192-200.

[2] Q. H. Wang, K. Kalantar-Zadeh, A. Kis, J. N. Coleman, M. S. Strano, *Nat. Nanotech.* **2012**, *7*, 699-712.

[3] A. K. Geim, I. V. Grigorieva, *Nature* **2013**, *499*, 419-25.

[4] K. Mak, C. Lee, J. Hone, J. Shan, T. F. Heinz, *Phys. Rev. Lett.* **2010**, *105*, 136805.

[5] A. Splendiani, L. Sun, Y. Zhang, T. Li, J. Kim, C. Chim, G. Galli, F. Wang, *Nano Lett.* **2010**, *10*, 1271-1275.

[6] B. Radisavljevic, A. Radenovic, J. Brivio, V. Giacometti, A. Kis, *Nat. Nanotechnol.* **2011**, *6*, 147-50.

[7] J. Feng, X. Qian, C. Huang, J. Li, *Nat. Photonics* **2012**, *6*, 866-872.

[8] M. Bernardi, M. Palummo, J.C. Grossman, *Nano Lett.* **2013**, *13*, 3664-3670.

[9] S. Kim, A. Konar, W. Hwang, J. K. Lee, J. Lee, J. Yang, C. Jung, H. Kim, J. Yoo, J. Choi, Y. Jin, S. Lee, D. Jena, W. Choi, Kinam. Kim, *Nat. Comm.* **2012**, *3*, 1-7.

[10] F. Withers, O. Del Pozo-Zamudio, A. Mishchenko, A. P. Rooney, A. Gholinia, K. Watanabe, T. Taniguchi, S. J. Haigh, A. K. Geim, A. I. Tartakovskii, K. S. Novoselov, *Nature Mater.* **2015**, *14*, 301-306.

[11] Z. Yin, H. Li, H. Li, L. Jiang, Y. Shi, Y. Sun, G. Lu, Q. Zhang, X. Chen, H. Zhang, *ACS Nano* **2011**, *6*, 74–80.

[12] Y. Yoon, K. Ganapathi, S. Salahuddin, *Nano Lett.* **2011,** *11*, 3768-3773

[13] A. K. Geim, *Science* **2009**, *324*, 1530–1534.

[14] F. Schwierz, *Nat. Nanotechnol.* **2010**, *5*, 487-96.

[15] H. Dery, H. Wu, B. Ciftcioglu, M. Huang, Y. Song, R. Kawakami, J. Shi, I. Krivorotov, I. Zutic, L.J. Sham, *IEEE Trans. Electron Devices* **2012**, *59*, 259-262.

[16] A. K. Geim, K. S. Novoselov, *Nature Mater.* **2007**, *6*, 183–191.

[17] S.H. Lee, D. Kim, J. Kim, G. Lee, J. Park, *J. Phys. Chem. C* **2009**, *113*, 21915-21920.

[18] X. Wan, G. Long, L. Huang, Y. Chen, *Adv. Mater.* **2011**, *23*, 5342–5358.

[19] Z. K. Liu, S. P. Lau, F. Yan, *Chem. Soc. Rev.* **2015,** *44*, 5638-5679.

[20] V. Shrotriya, G. Li, Y. Yao, C. Chu, Y. Yang, *Appl. Phys. Lett.* **2006**, *88*, 073508.

[21] A. Hadipour, D. Cheyns, P. Heremans, B. P. Rand, *Adv. Energy Mater.* **2011**, *1*, 930-935.

[22] A. Ayari, E. Cobas, O. Ogundadegbe, M. S. Fuhrer, *J. Appl. Phys.* **2007**, *101*, 014507.

[23] J. Kim, V. C. Tung, J. Huang, *Adv. Energy Mater.* **2011**, *1*, 1052-1057.

[24] J. C. Yu, J. Jang, B. Lee, G. Lee, J. Han, M. Song, *ACS Appl. Mater. Interfaces* **2014**, *6*, 2067-2073.

[25] Y. H. Chao, J. Wu, W. Jheng, C. Wang, C. Hsu, *Adv. Energy Mater.* **2013**, *3*, 1279-1285.

[26] J. J. Intemann, K. Yao, Y. Li, H. Yip, Y. Xu, P. Liang, C. Chueh, F. Ding, X. Yang, X. Li, Y. Chen, A. Jen, *Adv. Funct. Mater.* **2014**, *24*, 1465-1473.

[27] Q. V. Le, T. P. Nguyen, S. Y. Kim, *Phys. Status Solidi RRL* **2014**, *8*, 390-394.

[28] J. M. Yun, Y. Noh, J. Yeo, Y. Go, S. Na, H. Jeong, J. Kim, S. Lee, S. Kim, H. Koo, T. Kim, D. Kim, *J. Mater. Chem. C* **2013**, *1*, 3777.

[29] X. Gu, W. Cui, H. Li, Z. Wu, Z. Zeng, S. Lee, H. Zhang, B. Sun, *Adv. Energy Mater.*

2013, *3*, 1262-1268.

[30] W. Liu, X. Yang, Y. Zhang, M. Xu, H. Chen, *RSC Adv.* **2014**, *4*, 32744-32748.

[31] X. Yang, W. Fu, W. Liu, J. Hong, Y. Cai, C. Jin, M. Xu, H. Wang, D. Yang, H. Chen, *J. Mater. Chem. A* **2014**, *2*, 7727–7733.

[32] M. A. Ibrahem, T. lan, J. Huang, Y. Chen, K. Wei, L. Li., C. Chu, *RSC Adv.* **2013**, *3*, 13193-13202.

[33] Q. V. Le, T. Nguyen, K. Choi, Y. Cho, Y. Hong, S. Kim, *Phys. Chem. Chem. Phys.* **2014**, *16*, 25468–25472.

[34] M. J. Beliatis, K. K. Gandhi, L. J. Rozanski, R. Rhodes, L. McCafferty, M. R. Alenezi, A. S. Alshammari, C. A. Mills, K. D. G. I. Jayawardena, S. J. Henley, S. Ravi P. Silva, *Adv. Mater.* **2014**, *26*, 2078–2083.

[35] K. D. G. I. Jayawardena, R. Rhodes, K. K. Gandhi, M. R. R. Prabhath, G. Dinesha M. R. Dabera, M. J. Beliatis, L. J. Rozanski, S. J. Henley, S. Ravi P. Silva, *J. Mater. Chem. A* **2013**, *1*, 9922–9927.

[36] D. H. Wang, J. Kim, J. Seo, I. Park, B. Hong, J. Park, Alan. J. Heeger, *Angew. Chem., Int. Ed.* **2013**, *52*, 2874-2880.

[37] A. Castellanos-Gomez, L. Vicarelli, E. Prada, J. O. Island, K. L. Narasimha-Acharya, S. I. Blanter, D. J. Groenendijk, M. Buscema, G. A. Steele, J. V. Alvarez, H. W. Zandbergen, J. J. Palacios, H. S.J. van der Zant, *2D Mater.* **2014**, *1*, 025001.

[38] H. Liu, A. T. Neal, Z. Zhu, Z. Luo, X. Xu, D. Tománek, P. D. Ye, *ACS Nano* **2014**, *8*, 4033-4041.

[39] S. P. Koenig, R. A. Doganov, H. Schmidt, A. H. C. Neto, B. Özyilmaz, *Appl. Phys. Lett.* **2014**, *104*, 103106.

[40] M. Buscema, D. J. Groenendijk, S. I. Blanter, G. A. Steele, H. S.J. van der Zant, A. Castellanos-Gomez, *Nano Lett.* **2014**, *14*, 3347-52.

[41] P. Yasaei, B. Kumar, T. Foroozan, C. Wang, M. Asadi, D. Tuschel, J. E. Indacochea, R.

F. Klie, A. Salehi-Khojin, *Adv. Mater.* **2015**, *27*, 1887-1892.

[42] J. Kang, J. D. Wood, S. A. Wells, J. Lee, X. Liu, K. Chen, Mark. C. Hersam, *ACS Nano* **2015**, *9 (4)*, 3596-3604.

[43] D. Hanlon, C. Backes, E. Doherty, C. S. Cucinotta, N. C. Berner, C. Boland, K. Lee, P. Lynch, Z. Gholamvand, A. Harvey, S. Zhang, K. Wang, G. Moynihan, A. Pokle, Q. M. Ramasse, N. McEvoy, W. J. Blau, J. Wang, S. Stefano, D. D. ORegan, G. S. Duesberg, V. Nicolosi, J. N. Coleman, *arXiv* **2015**, *1501*, 01881.

[44] a) Y.Q. Cai, Q.Q. Ke, G. Zhang, Y.P. Feng, V.B. Shenoy, Y.W. Zhang, *Adv. Funct. Mater.* **2015**, *25*, 2230-2236. b) R. X. Fei and L. Yang, *Appl. Phys. Lett.* **2014**, 105, 083120.

[45] S. Zhang, J. Yang, R. Xu, F. Wang, W. Li, M. Ghufran, Y. Zhang, Z. Xu, G. Zhang, Q. Qin, Y. Lu, *ACS Nano* **2014**, *8*, 9590-9596.

[46] S. Liu, P. You, J. Li, J. Li, C. Lee, B. S. Ong, C. Surya, F. Yan, *Energy Environ. Sci*. **2015**, *8*, 1463.

[47] Z. He, C. Zhong, S. Su, M. Xu, H. Wu, Y. Cao, *Nat. Photon.* **2012**, *6*, 591.

[48] Z. K. Liu, J. H. Li, Z. H. Sun, G. A. Tai, S. P. Lau, F. Yan, *ACS Nano* **2012**, *6*, 810.

[49] M.F. Lo, Z.Q. Guan, T.W. Ng, C.Y. Chan, C.S. Lee, *Adv. Funct. Mater.* **2015**, *25*, 1213-1218.

[50] Y.Q. Cai, G. Zhang, Y.W. Zhang, *Sci. Rep.* **2014**, 4, 6677.

[51] D, Xiang, C. Han, J. Wu, S. Zhong, Y.Y. Liu, J.D. Lin, X.A. Zhang, W.P. Hu, B. Özyilmaz, A.H. C. Neto, A. T. S. Wee, W. Chen, *Nat. Commun.*, **2015**, 6, 6485.

[52] Y. Cai, Q. Ke, G. Zhang, and Y.-W. Zhang, *J. Phys. Chem. C* **2015**, 119, 3102.

Figures:

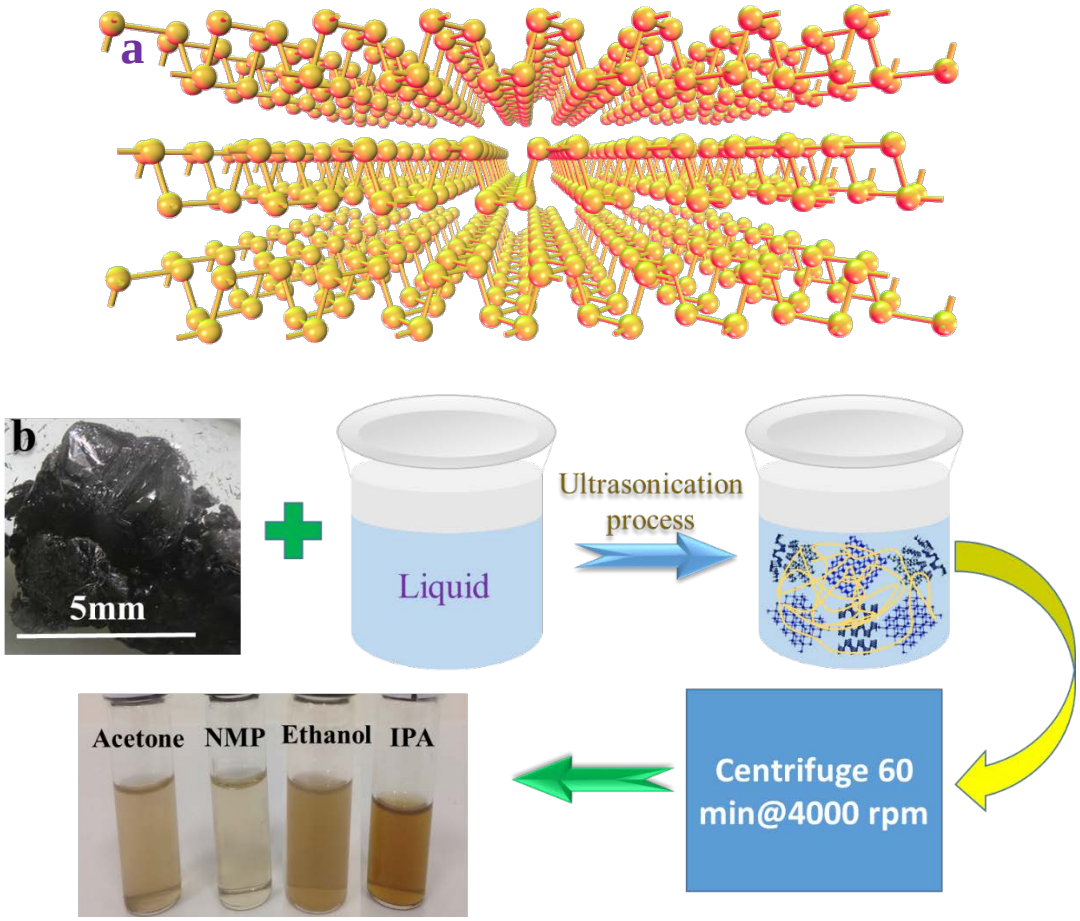

Figure 1. **a**) Schematic crystal structure of BP. **b**) Photograph of a BP crystal. Illustrations of the ultrasonication process of BP solution. Photograph of the exfoliated BP in acetone, IPA, ethanol and NMP solvents.

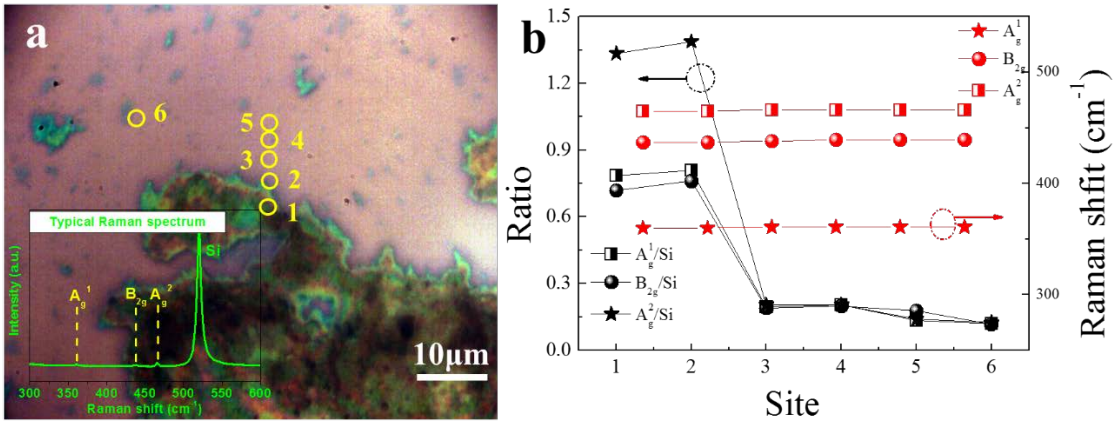

Figure 2. **a**) Optical image of the BP flakes drop-casted onto SiO_2/Si substrate. The BP flakes at six different locations are indicated. The inset shows a typical Raman spectrum of the BP flake at site 3. **b**) The Raman shift of the three BP modes measured at different sites. Raman intensity ratios of A^1_g, B_{2g}, and A^2_g to Si modes measured at various sites.

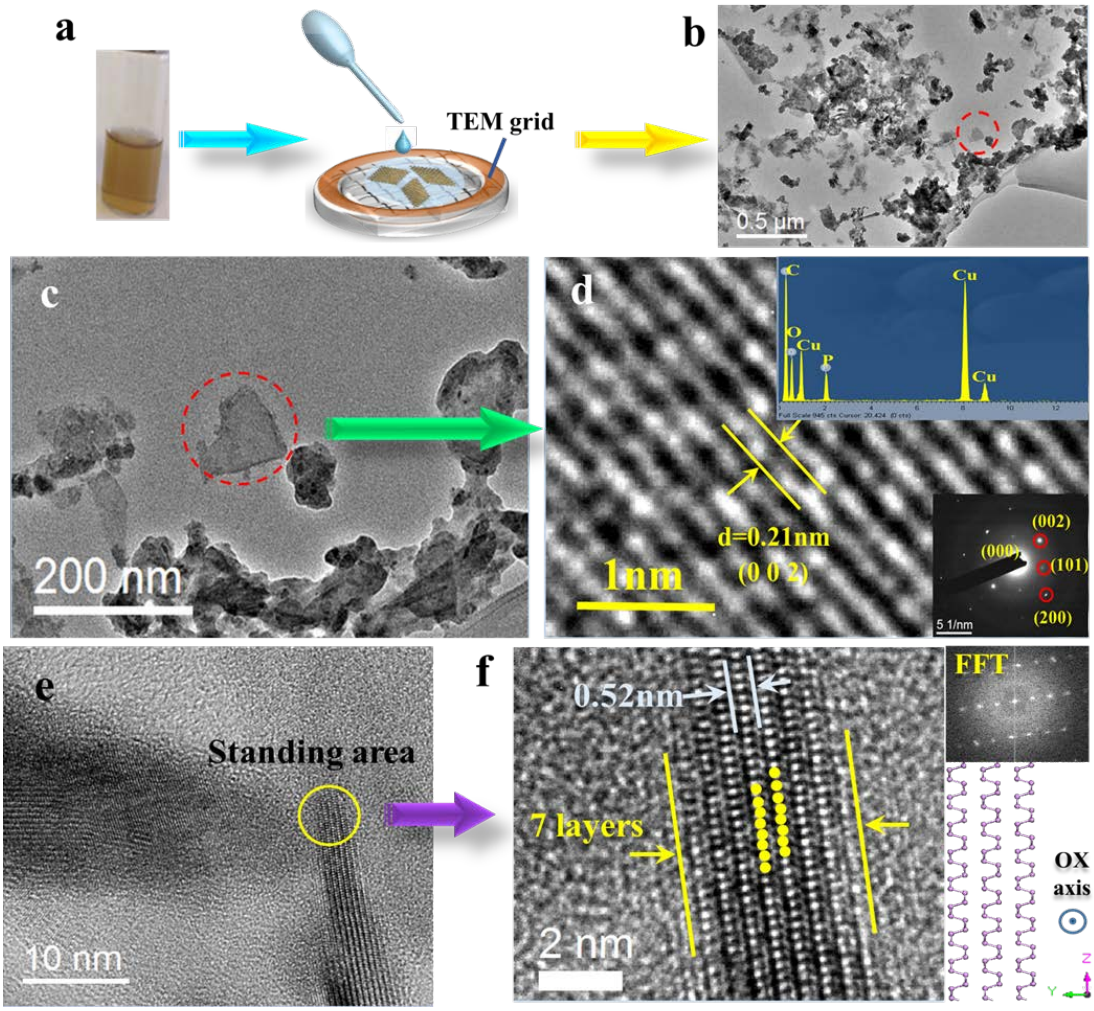

Figure 3. **a**) Schematic illustration of the BP solution drop-casted onto a TEM grid. **b**) A typical TEM image of BP flakes prepared in IPA solution. **c**) Local zoom-in of the area marked in (b) with a red dash circle. **d**) HRTEM image of the BP flake mentioned in **c**. The insets show the corresponding SAED pattern and EDX result. **e**) HRTEM image of a BP showing layered structure. **f**) Zoom-in HRTEM image of the BP as indicated **e** and the corresponding FFT image (top, right) and simulated layered structure (bottom, right) along *OX* axis.

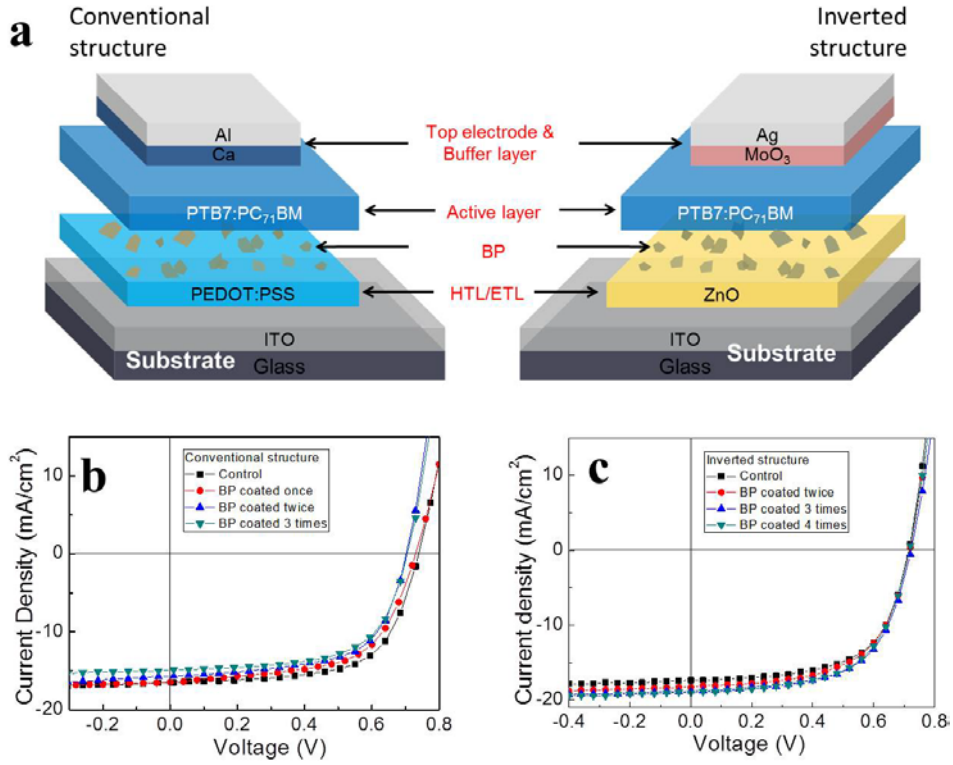

Figure 4. **a**) Conventional and inverted architectures of OPVs based on PTB7/$PC_{71}BM$; J-V characteristics of **b)** conventional, and **c** inverted OPVs with BP incorporation under different conditions.

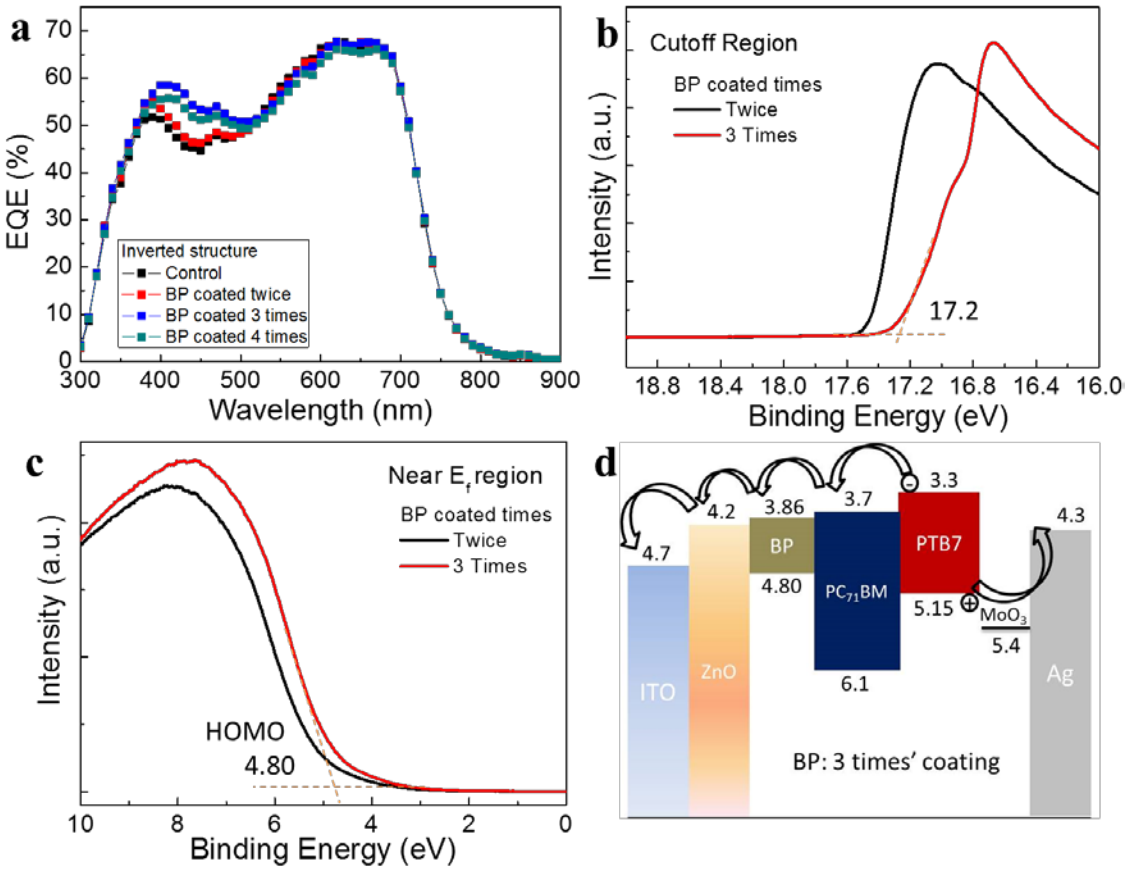

Figure 5. **a)** EQE characteristics of a control device and the inverted OPVs with the incorporation of BP spin coated for different times. UPS (He I) spectra of **b)** the cutoff region and **c)** the near Fermi energy region of the BP spin coated on Si substrates for 2 or 3 times. **d**) Energy band structure of the OPV based on PTB7/PC71BM with the incorporation of BP (3 times' coating).